PNAS RESEARCH ARTICLE | BIOPHYSICS AND COMPUTATIONAL BIOLOGY

Targeted NMR signal enhancement of RNA by site-directed bis-nitroxide labeling

Rubin Dasgupta[a,1], Christian Steinmetzger[a,1], Ancy T. Wilson[b,1], Satyaki Chatterjee[b], Gunnar W. Reginsson[b], Snorri Th. Sigurdsson[b,2], and Katja Petzold[a,2]

Affiliations are included on p. 7.

Edited by Joseph D. Puglisi, Stanford University School of Medicine, Stanford, CA; received November 4, 2025; accepted February 12, 2026

MicroRNAs regulate gene expression through sequence-specific interactions with target messenger RNAs (mRNAs), and their misregulation is a hallmark of cancer. MicroRNA-34a (miR-34a), a key modulator of the tumor suppressor p53, binds the mRNA encoding sirtuin 1 (mSirt1) and adopts multiple conformational states that influence repression efficiency. While such dynamics have been characterized in vitro, extending these studies to cellular environments is hampered by weak signals and substantial background inherent to nucleic acid NMR. To overcome this limitation, we developed a site-directed spin labeling strategy for RNA that enables targeted dynamic nuclear polarization (DNP) signal enhancement. Using the bisnitroxide polarizing agent AsymPol-NCS-SDSL, we conjugated spin labels to specific positions of mSirt1 RNA and annealed them to $^{13}C,^{15}N$-cytidine-labeled miR-34a. At 9.4 T, we observed up to 27-fold signal enhancements. The selectivity of polarization transfer within the RNA duplex relative to the surrounding environment could be tuned by matrix deuteration, while doping with paramagnetic metal ions accelerated polarization build-up times, with Cu^{II} proving more efficient than Gd^{III}. This work establishes bisnitroxide-based SDSL as a powerful approach for targeted DNP of nucleic acids, enabling high-sensitivity studies of nucleic acids at concentrations ≤40 μM and paves the way for structural investigations of microRNA–mRNA interactions in cells.

RNA | site-directed spin labeling | targeted DNP | AsymPol | NMR spectroscopy

MicroRNAs are central modulators of gene expression and their misregulation is linked to numerous diseases including cancer (1). Among them, microRNA 34a (miR-34a), a 22 nucleotide long regulatory RNA, is frequently downregulated in tumors and plays a pivotal role in controlling the tumor suppressor protein p53 via a feedback loop (2–4). While miR-34a is directly regulated by p53, it indirectly acts on p53 via targeting the mRNA of the silent information regulator (SIRT1, here called mSirt1), a deacetylase of p53. It has recently been shown that miR-34a can adopt multiple conformations when bound to the mSirt1 transcript. A minor conformational state, discovered by NMR spectroscopy, displays enhanced repression efficiency (2, 5). This excited state is populated 1% in vitro, but interpretations of the effect in human cells are challenging to ascertain without knowing, e.g., the population of this state in the cell. Furthermore, how microRNA in general, and specifically miR-34a, select their specific targets from a pool of over 100 targets (2–4), depends on several, environmentally defined, factors, such as ions, mRNA structure, etc. While these biophysical, structural, and dynamic behaviors have been observed in vitro, extending such analyses to cellular environments remains essential both for understanding mRNA function and for developing microRNA-based therapeutics (6).

In-cell NMR has enabled the structural characterization of proteins and nucleic acids within the highly crowded cellular environment, which contains approximately 300 g/L of proteins, 100 g/L of RNA as well as ions and metabolites at a total concentration of around 300 mM (7, 8). When using conventional solution-state techniques for in-cell NMR, millimolar concentrations of the target biomolecules are required, which can be achieved through overexpression (7, 8) or electroporation (9–11) into cells. Such concentrations exceed typical physiological levels and may compromise the biological relevance of the resulting structural information, while still suffering from spectral crowding with the dense molecular environment of the cell. Therefore, structural and biophysical characterization of microRNA–mRNA interactions in cells continue to pose technical challenges.

Solid-state NMR, combined with dynamic nuclear polarization (DNP) enhancement of signals, offers a powerful tool to probe nucleic acid structures and dynamics at low concentrations (5, 6, 12). DNP transfers the large polarization of unpaired electrons in

Significance

Understanding RNA structure and dynamics inside cells remains a key challenge in molecular biology. Here, we establish a site-directed spin labeling approach that enables targeted NMR signal enhancement of RNA in complex environments, using dynamic nuclear polarization (DNP) to remove all background. By attaching the bisnitroxide radical AsymPol to defined RNA sites, we achieved 27-fold signal increase and provide proof-of-concept for tunable and local sensitivity enhancement. This strategy provides a broadly applicable route for highly sensitive, site-specific NMR analysis of RNA or RNA complexes at physiological concentrations, paving the way for structural and biophysical investigations of RNA regulatory mechanisms within their complex native environments. We demonstrated the feasibility on the cancer gatekeeper regulator microRNA-34a targeting the mRNA of sirtuin 1.

Preprint servers: This manuscript was deposited as a preprint to ChemRxiv (DOI: 10.26434/chemrxiv-2025-1tkv0) under a CC BY-NC-ND 4.0 license.

The authors declare no competing interest.

This article is a PNAS Direct Submission.

[1]R.D., C.S., and A.T.W. contributed equally to this work.

[2]To whom correspondence may be addressed. Email: snorrisi@hi.is or katja.petzold@imbim.uu.se.

This article contains supporting information online at https://www.pnas.org/lookup/suppl/doi:10.1073/pnas.2531087123/-/DCSupplemental.

Published March 18, 2026.

so-called polarizing agents (PAs), commonly bis-nitroxides, that are added to the sample of interest. The most effective mechanism of polarization transfer is the cross effect (CE), an electron–electron–nuclear three-spin interaction that first generates polarization on atomic nuclei surrounding the PA before it propagates through the matrix to the sample by spin diffusion (13). Under magic-angle spinning (MAS) and microwave (μw) irradiation, an NMR-observable nuclear magnetization with greatly enhanced sensitivity (up to 660-fold enhancement) over thermal equilibrium magnetization can subsequently be observed through DNP (14). This has enabled studies of membrane proteins (15), amyloid fibrils (16), and intrinsically disordered proteins (17), both in vitro and in cells. Furthermore, it has enabled the detection of sparse conformational states and key interactions in isolated nucleic acids (18, 19) as well as nucleic acid–protein complexes (5, 20). Moreover, DNP has facilitated detection of biomolecules such as ubiquitin (21, 22), the yeast prion protein Sup35NM (23) and G-quadruplex-forming nucleic acids (24) at low concentrations in native cellular environments (25). However, conventional DNP uses PA concentrations on the order of 10 mM (5, 26) and enhances both target and background signals, which limits its applicability for more detailed, selective RNA studies in complex mixtures.

Targeted DNP approaches address this limitation by using PAs attached to the biomolecule of interest. Site-directed spin labeling (SDSL) is a technique that has been extensively used to incorporate spin labels at specific sites in proteins (27, 28). Indeed, proteins that contain nitroxide monoradicals, incorporated by SDSL, have been used for MAS-DNP (29). Proteins were subjected to SDSL using nitroxide biradicals via conjugation of cysteine with methanethiosulfonate (29, 30) or maleimide (31) derivatives of AMUPol or TOTAPOL (*SI Appendix*, Table S1). Furthermore, amber codon suppression has been used to introduce an unnatural norbornene amino acid into ubiquitin followed by a click reaction with a tetrazine derivative of TOTAPOL (32). Alternatively, noncovalent binding of TOTAPOL-modified high-affinity ligands to dihydrofolate reductase has been demonstrated to directly yield promising levels of polarization enhancement (33) or generate localized paramagnetic relaxation enhancement (PRE) that is read out via difference spectroscopy (*Sel*DNP) (34). Additionally, paramagnetic metal ions such as Gd^{3+} and Mn^{2+}, that can operate via the solid effect (SE) DNP mechanism and directly polarize atomic nuclei in the sample, have been used for DNP enhancement. By attaching a maleimide derivative of the chelating ligand DOTA to cysteines in ubiquitin and binding to Gd^{3+}, direct polarization of ^{13}C and ^{15}N via SE DNP yielded absolute enhancement factors of 9× and 100×, respectively (35, 36).

To date, only two studies have demonstrated targeted DNP in nucleic acids, both relying on direct SE polarization of ^{13}C with Mn^{2+} that replaced natively bound Mg^{2+} in a hammerhead ribozyme to obtain enhancement factors up to 8× (37, 38). Given that suitable high-affinity metal ion binding sites at desired locations are not universally present in nucleic acids (39), there is a clear need for further development of targeted DNP methodology for nucleic acids. With the advances made in nitroxide biradical PAs for CE DNP (40–42) and the growing recognition of RNA as a key player in biology (43, 44), development of new strategies optimized for specific DNP applications is of paramount importance and content of this work.

Here, we report a SDSL approach in which a DNP-active nitroxide biradical is covalently linked to an RNA for targeted DNP. Specifically, an isothiocyanate derivative of the highly effective PA AsymPol (45) was conjugated to 2′-amino groups of RNA using established RNA modification chemistry (46, 47). Four spin-labeled fragments of mSirt1 were annealed to isotope-labeled miR-34a and subsequent DNP NMR yielded enhancement factors ($\varepsilon_{on/off}$) of up to 27×. In proton-rich environments, the enhancement is dispersed between RNA molecules due to distance-dependent, environment-mediated spin diffusion. We show that the degree of localization can be tuned from a global enhancement to a more selective, albeit slightly reduced enhancement by increasing the degree of deuteration of the surrounding matrix. We observed long build-up times (T_B) for transferring spin polarization of the PA to detectable magnetization on the RNA that could be reduced using paramagnetic metal ions. These results demonstrate that nitroxide biradical-based SDSL can deliver targeted MAS-DNP in RNA and open the door to high-sensitivity studies of microRNA–mRNA complexes in cellular environments.

Results

Synthesis of AsymPol Isothiocyanate for RNA Conjugation. To enable SDSL of RNA with a DNP-active biradical, we designed and synthesized a reactive derivative of the PA AsymPol suitable for conjugation to defined positions within RNA. Aromatic isothiocyanates react readily and selectively under mild conditions with 2′-amino-groups in RNA, shown not to significantly perturb RNA structure (48, 49) and are, therefore, ideal reagents for SDSL (46, 50). The required 2′-amino-containing nucleotides can be introduced at specific sites either by solid-phase synthesis using known phosphoramidite building blocks (51–53) or by enzymatic methods (54). For 5′- and 3′-terminal functionalization of RNA, alkylamino solid supports and amino-modified phosphoramidites are available. Therefore, we prepared AsymPol-NCS-SDSL (Scheme 1) for covalent and SDSL of amino-modified RNA with AsymPol.

The synthesis of **AsymPol-NCS-SDSL** started with a condensation of **1** with **2** to yield monospirocycle **3**, followed by oxidation to give nitroxide radical **4** (Scheme 1). Reductive amination to yield **5** was followed by conjugation with 3-carboxy-pyrrolinoxyl nitroxide **6** (55) and gave **7**, which was hydrolyzed to the corresponding carboxylic acid **8**. Subsequent coupling with 4-aminobenzylamine and reaction with thiophosgene yielded **AsymPol-NCS-SDSL** in a total of seven steps.

Although this scheme describes an AsymPol derivative for conjugation to 2′-amino RNA, it represents a general strategy. First, the AsymPol-carboxylic acid **8** can be modified with functional groups other than isothiocyanates for different conjugation chemistry. Second, introduction of the aminobenzyl linker with standard amide coupling chemistry and conversion to the relatively stable and easy to handle aromatic isothiocyanate group at a late stage makes the strategy compatible with other PAs. This synthesis provides a robust and versatile route to AsymPol functionalization, yielding an isothiocyanate derivative that enables covalent site-specific labeling of RNA, establishing the foundation for targeted DNP studies of nucleic acids.

RNA Conjugation. To evaluate the efficiency and versatility of AsymPol-NCS-SDSL for targeted RNA labeling, we conjugated it to defined sites within mSirt1 representing distinct structural contexts. AsymPol was introduced at four different sites in synthetic mSirt1 analogs (**S1–S4**) representing base-paired and bulged regions (Fig. 1*A* and *SI Appendix*, Table S2). **AsymPol-NCS-SDSL** was reacted with **S1–S4** in borate buffer for 4 to 8 h at 37 °C as described previously (Fig. 1*A*) (46). Excess spin labeling reagent and any unreacted starting RNA that might have been produced by transamidation of the aliphatic amino groups

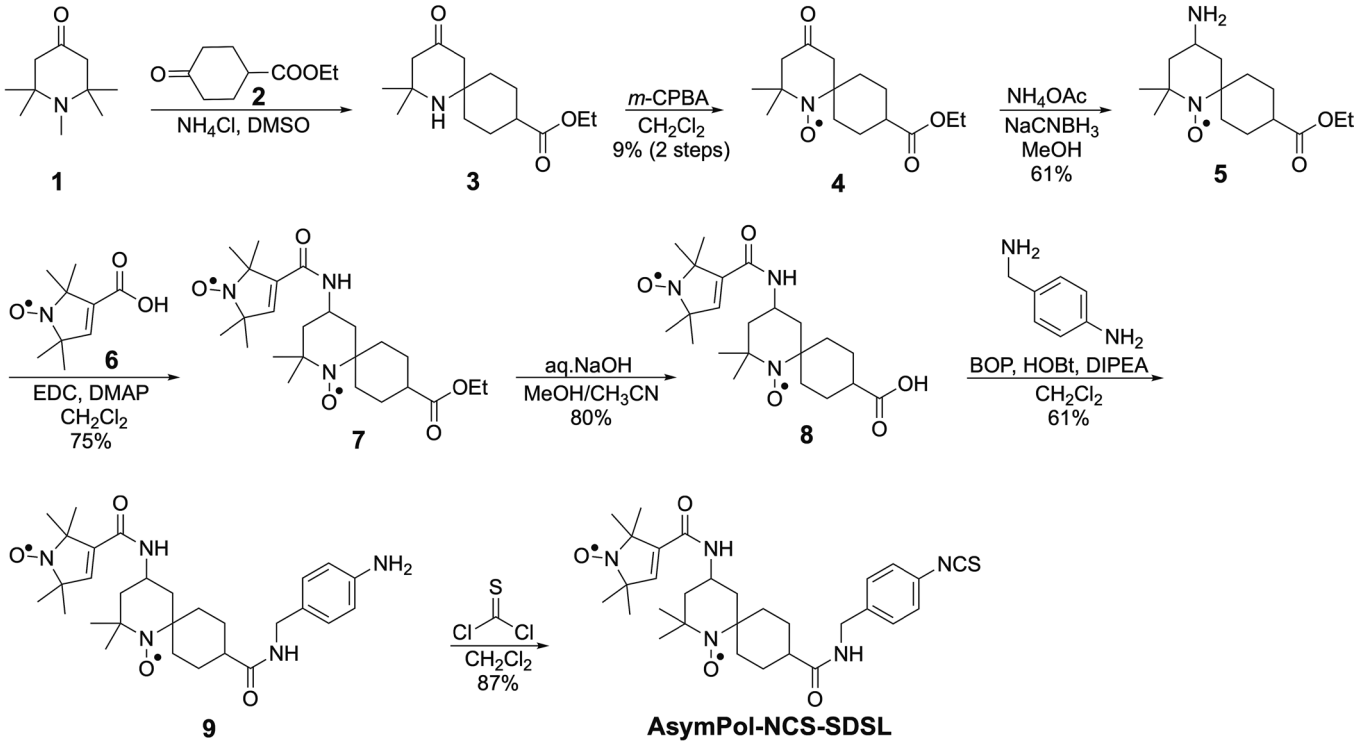

Scheme 1. Synthesis of the bis-nitroxide **AsymPol-NCS-SDSL** for SDSL of amino-modified RNA. Full experimental details are given in *SI Appendix*.

during solid-phase synthesis were removed by standard denaturing polyacrylamide gel electrophoresis (PAGE) purification. Electron paramagnetic resonance (EPR) spectra of the AsymPol-conjugated mSirt1 (**S1***–**S4***) showed partial reduction of the biradical to a monoradical, which reduces the DNP-active RNA-labeled fraction to 10 to 20%. This was accounted for by deconvolution of the proportion of bi- and monoradicals (*SI Appendix*, Fig. S1 and additional discussion in *SI Appendix*, section 1.4). The available amount of biradical-modified RNA is thus equivalent to typical working concentrations of exogenously transfected nucleic acids in solution-state in-cell NMR experiments (11). Therefore, we proceeded with sample preparation for DNP NMR. Spin-labeled **S1***–**S4*** was annealed with ^{13}C,^{15}N-cytidine-labeled miR-34a [**M**^{C}, transcribed from a tandem repeat plasmid as reported previously (5)] to produce RNA duplexes that accommodate the PA in base-paired, open bulged or dangling structural contexts and at various distances to the isotope-labeled nucleotides (Fig. 1*B*).

DNP-Enhanced NMR Spectroscopy. To assess the performance of AsymPol-labeled RNA in DNP MAS NMR, we compared signal enhancements and structural integrity across spin-labeled miR-34a:mSirt1 duplexes under optimized experimental conditions. While previous DNP experiments on the mSirt1:miR-34a duplex were performed with isotopically labeled guanosine (5), cytidine labeling was used here to reduce spectral complexity (three C vs. eight G nucleotides) and to avoid ^{13}C signal overlap with spinning side bands from MAS at 11 kHz. The biradical-conjugated RNA duplexes (**M**^{C}**S***, Fig. 1*B* and *SI Appendix*, Table S3) were dissolved at a concentration of 20 to 40 μM in a matrix comprising 60% $^{12}C_3$,$^{2}H_8$-glycerol, 40% H_2O, and 175 mM each of trehalose and mannitol, referred to as "DNP nectar," which provides higher DNP enhancement factors compared to conventional "DNP juice" (5, 56). DNP experiments were conducted with ~8 to 16 μg (0.5 to 1 nmol) of biradical-conjugated RNA in 3.2 mm rotors at 400 MHz ^{1}H frequency, 263 GHz gyrotron frequency, with 11 to 12 kHz MAS frequency at 102 to 110 K. The presence of monoradicals due to partial reduction of the biradical can result in PRE and thus affect CE polarization transfer (57–61). However, due to long intermolecular distances (on the order of 10 to 20 nm, see also below), this effect will be negligible. Therefore, the observed signal enhancement and polarization build-up times can be fully attributed to the biradical-bearing fraction of the RNA. Full details of the spin labeling conditions, sample preparation, and NMR experiments are given in the supporting information.

^{1}H–^{13}C cross polarization (CP) MAS experiments yielded enhancement factors ($\varepsilon_{on/off}$) in the range of 5× to 27×, with the strongest enhancement observed for **M**^{C}**S2*** and **M**^{C}**S3*** (Fig. 2 and *SI Appendix*, Table S4). The enhancement factor can vary by ~21% between sample preparations for the same duplex, which can be attributed to rotor packing with the highly viscous DNP nectar (*SI Appendix*, Tables S4 and S5). Nucleobase carbon atoms C2, C4, and C6 were directly observed and agree with results for unmodified RNA under conventional DNP conditions (*SI Appendix*, Fig. S5), while ribose C1′ to C5′ and nucleobase C5 were not visible due to signal background from trehalose and mannitol. Background removal by means of a ^{15}N–^{13}C zTEDOR experiment (62) revealed the N1-bound anomeric C1′ resonance (*SI Appendix*, Fig. S3). Together with unchanged chemical shifts of nucleobase nitrogen atoms N1, N3, and N4 in ^{1}H–^{15}N CP MAS spectra (*SI Appendix*, Fig. S4), no significant structural perturbation was observed for the covalent attachment of the PA. The average build-up time of steady-state nuclear polarization under μw irradiation ($T_{B,on}$) is 24 ± 3 s for the four duplexes, as determined by saturation recovery of the bulk ^{1}H signal (*SI Appendix*, Fig. S6); optimal signal-to-noise per unit time is obtained when the interscan delay equals 1.3 × $T_{B,on}$ (63). For AsymPol-POK, a water-soluble derivative of AsymPol, $T_{B,on}$ = 1.5 s has been determined at a PA concentration of 10 mM in DNP juice under comparable

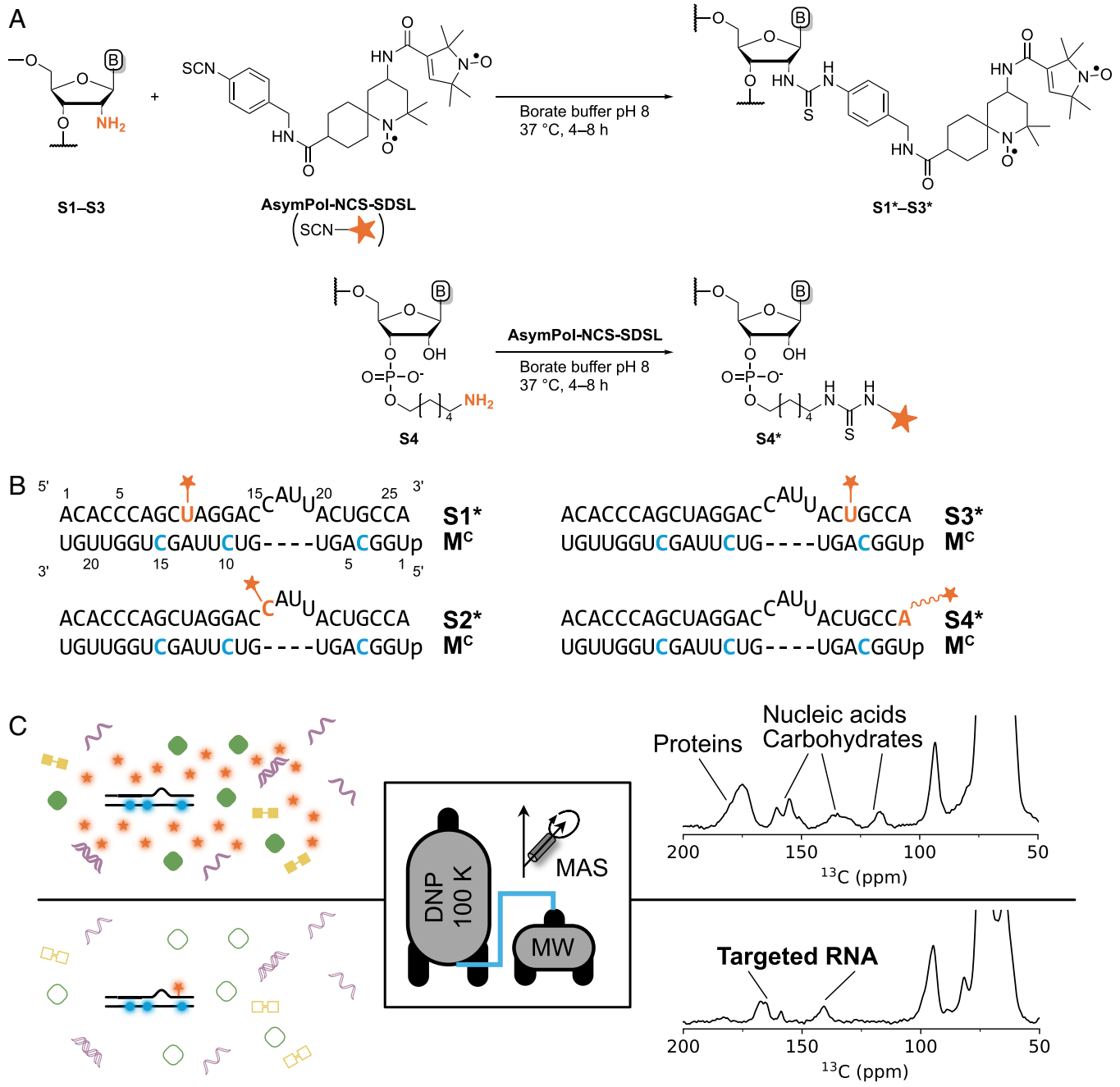

Fig. 1. (*A*) Conjugation of amino-modified RNA with **AsymPol-NCS-SDSL** (full experimental details in *SI Appendix*). B denotes the nucleobase (here: C/U for **S1–S3**, A for **S4**). (*B*) Secondary structure of modified mSirt1 fragments **S1*–S4*** (*Top* strands) hybridized with miR-34a (**M**^{C}, *Bottom* strands). ^{13}C,^{15}N-cytidine isotope labeling is indicated in blue. Attachment sites for spin labeling are highlighted in orange. A wavy line denotes 3′-terminal attachment with a hexylamino linker for **S4***. (*C*) *Top*: Under conventional DNP conditions, resonances from an RNA of interest (blue) can be obscured by those from other, more abundant, sample constituents such as proteins, carbohydrates, and interfering nucleic acids (green, yellow, violet) that are also enhanced by the PA (orange). *Bottom*: By SDSL the RNA of interest with the PA, a targeted enhancement over the background is achieved.

experimental conditions (45). Here, the concentration of AsymPol is equal to that of the biradical-conjugated RNA at 20 to 40 μM, resulting in a >250-fold decrease in concentration and a 16-fold increase in $T_{B,on}$. This inverse relationship between PA concentration and $T_{B,on}$ is well known (57, 64–69) and the present findings qualitatively match reports of some nitroxide monoradicals for which a 40-fold decrease in concentration increases $T_{B,on}$ 8 to 12-fold (70). These results demonstrate that covalent attachment of AsymPol enables substantial DNP enhancement without detectable perturbation of RNA structure, establishing the feasibility of targeted hyperpolarization at low RNA concentrations.

The Role of Spin Diffusion. In CE MAS DNP, electron polarization is first transferred to ^{1}H nuclei with strong hyperfine coupling to the biradical, from where it moves outward and then rapidly propagates into the bulk of the sample by spin diffusion (13, 71). Recent experimental studies, combined with numerical simulations, show that in the case of AsymPol-type PAs, the initial polarization transfer proceeds to ^{1}H spins in the matrix rather than those directly bonded to the PA (72). In order for targeted DNP to produce signal enhancement that remains confined to the vicinity of the spin-labeled biomolecule and thus minimize polarization leakage to unwanted sample constituents, spin diffusion must be controlled.

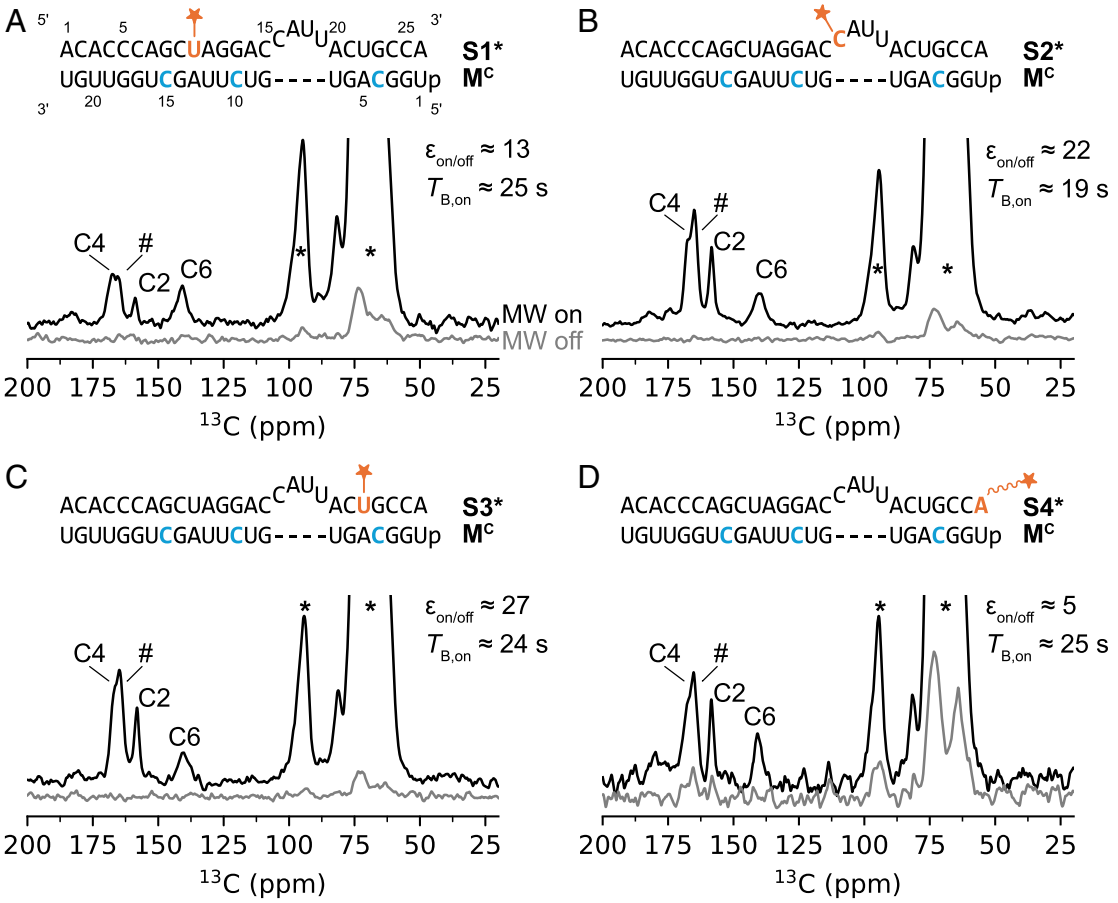

Fig. 2. ^{1}H–^{13}C CP MAS spectra (3 ms τ_{CP}) of (*A*) **M^{C}S1***, (*B*) **M^{C}S2***, (*C*) **M^{C}S3***, (*D*) **M^{C}S4*** in DNP nectar with (black) or without (gray) μw irradiation. $\varepsilon_{on/off}$ was determined from the signals between 50 and 110 ppm. $T_{B,on}$ was measured by saturation recovery. Asterisks (*) denote background from natural isotopic abundance trehalose and mannitol, which overlaps with the ribose C1′ to C5′ and nucleobase C5 resonances. # indicates an unassigned background signal.

To investigate spin diffusion, the biradical was separated from the isotope label by preparing a sample of two mixed RNA duplexes containing 26 μM each of 1) natural abundance miR-34a hybridized with U22-spin-labeled mSirt1 (**MS3***) and 2) ^{13}C,^{15}N cytidine-labeled miR-34a hybridized with non-spin-labeled mSirt1 (**M^{C}S5**) (Fig. 3). At this concentration, the average distance between duplex molecules is on the order of 10 to 20 nm (Wigner–Seitz radius). A ^{1}H–^{13}C CP MAS spectrum in DNP nectar [40% H_2O, 180 mM each of trehalose and mannitol, [^{1}H] = 48 M] shows significant signal enhancements for the C2, C4, and C6 resonances of cytidine in one duplex from the AsymPol spin labels in the other duplex, which we attribute to spin diffusion. $T_{B,on}$ of the bulk ^{1}H polarization in the mixed sample was unchanged from the values reported in *SI Appendix*, Table S5, while $\varepsilon_{on/off}$, which mainly reports on glycerol, trehalose, and mannitol signals, had decreased by 48% with respect to **M^{C}S3*** (Fig. 3*A*). Exchanging H_2O to D_2O [final [^{1}H] = 4 M] greatly reduces spin diffusion and consequently prevents polarization transfer between the mixed duplexes, leading to no observable signal from the isotope-labeled RNA (Fig. 3*B*). For the nonmixed duplex **M^{C}S3***, reducing [^{1}H] from 48 M to 15 M (DNP nectar with 10% H_2O, 30% D_2O) has no discernible effect on $\varepsilon_{on/off}$ or the relative intensity of RNA resonances over the background (Fig. 3*C*), but increased $T_{B,on}$ to 30.4 ± 0.1 s. This level of matrix deuteration is equivalent to conventional DNP juice [[^{1}H] = **11** M], which is optimal for nontargeted DNP (73), indicating that there is still spin diffusion present. At [^{1}H] = **4** M in DNP nectar, however, background signals are greatly diminished while the nucleobase carbon resonances are less affected Fig. 3*D* and $T_{B,on}$ of the bulk ^{1}H polarization remains at 31.7 ± 2.2 s. Improved localization with a concomitant increase in $T_{B,on}$ has also been observed in targeted protein hyperpolarization with a TOTAPOL-modified peptide ligand bound to its target protein in a perdeuterated matrix (31). Therefore, it would be expected that localization of the polarization enhancement to miR-34a:mSirt1 RNA duplexes would benefit from complete deuteration of the matrix. These findings confirm that matrix deuteration effectively confines polarization to the spin-labeled RNA, reducing background signal while preserving the RNA signal, an essential step toward achieving target-selective DNP in complex environments.

Doping with Paramagnetic Metal Ions. To explore strategies for accelerating polarization build-up and improving overall sensitivity, we examined the effect of paramagnetic metal ions on the DNP performance of AsymPol-labeled RNA. High $T_{B,on}$ necessitates a long recovery time and, therefore, limits the amount of signal per unit time that is possible to acquire. The sensitivity of targeted DNP may be improved by employing a higher concentration of PA-conjugated RNA to reduce $T_{B,on}$ (64). While this approach is feasible in vitro, it might not be possible when working with limited amounts of RNA in cells. Therefore, we investigated whether paramagnetic dopants, such as Cu^{II} or Gd^{III}, could be exploited to increase the sensitivity of targeted DNP. In a recent study, addition of up to 8 mM Gd^{III}HP-DO3A was shown to increase ^{13}C hyperpolarization of isotope-labeled glucose by trityl radicals at 1.1 K (74). $Cu^{II}Na_2EDTA$,

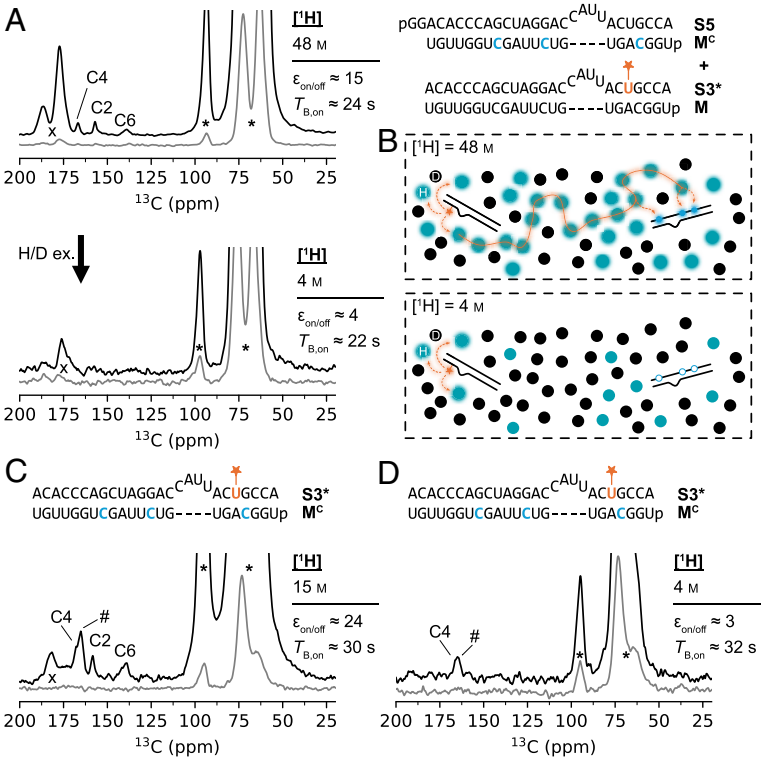

Fig. 3. (*A*) ^{1}H–^{13}C CP MAS spectra (3 ms τ_{CP}) of mixed RNA duplexes **MS3*** + **M^{C}S5** in DNP nectar (40% H_2O, 180 mM each of trehalose and mannitol) with (black) or without (gray) μw irradiation. The proton concentration in the matrix is 48 M. After D_2O exchange of the labile protons, the residual proton concentration had been reduced to 4 M and no intermolecular polarization transfer between duplexes was observed. (*B*) Spin diffusion was efficient at high proton concentration (cyan) and propagates ^{1}H polarization throughout the matrix (orange), resulting in intermolecular signal enhancement. At lower proton concentrations, this effect was strongly attenuated. (*C*) For the spin-labeled duplex **M^{C}S3***, a proton concentration of 15 M (10% H_2O, 30% D_2O) has little effect on signal intensity (compare Fig. 2*C*). (*D*) At 4 M proton concentration (40% D_2O), prominence of the RNA signals over the matrix has increased and enhancement decreased. Asterisks denote background from natural isotopic abundance glycerol, trehalose, and mannitol. x denotes spinning sidebands of background signals. # indicates an unassigned background signal.

on the other hand, has been mainly employed in conventional solid-state NMR to reduce ^{1}H longitudinal relaxation times and therefore enable shorter interscan delays (75, 76). Samples of the RNA duplex **M^{C}R3*** in DNP nectar were titrated with either $Cu^{II}Na_2EDTA$ up to 30 mM (Fig. 4 *A* and *B*) or $Gd^{III}DOTA$ up to 6.1 μM (Fig. 4 *C* and *D*). While $T_{B,on}$ was reduced with increasing dopant concentrations as anticipated, this was accompanied by a significant reduction in $\varepsilon_{on/off}$ (Fig. 4*E* and *SI Appendix*, Table S5), especially for cytidine C6, where resonances became unobservable at the highest concentrations of paramagnetic dopants. Thus, DNP sensitivity was not enhanced and is in line with previously reported values (57). Interestingly, the achievable signal-to-noise per unit time was unchanged when doping with Cu^{II} (Fig. 4*F*), indicating that it might be possible to identify paramagnetic metal ions with favorable properties for DNP NMR, where reduction in the interscan delay is larger than reduction of the signal enhancement. While extended experiment durations due to long $T_{B,on}$ times currently remain a limitation of the presented approach for dilute samples, future improvements of these initial doping experiments can potentially lead to sensitivity gains with different metal ions.

Discussion

In summary, we established that **AsymPol-NCS-SDSL** enables targeted DNP MAS NMR of RNA. Conjugation of this isothiocyanate derivative of AsymPol to amino-modified RNA was achieved under mild conditions. This strategy is generally adaptable, allowing spin-labeling with other PAs or employing alternative labeling chemistries when isothiocyanates are not suitable.

Using spin-labeled mSirt1 mRNA fragments hybridized with ^{13}C,^{15}N-cytidine labeled miR-34a, we observed DNP enhancements of up to 27-fold (Figs. 1 and 2). At the low RNA/biradical concentration of 20 to 40 μM used in the present study, sensitivity was limited by bulk ^{1}H polarization build-up times. Paramagnetic doping with Gd^{III} did not enhance the DNP sensitivity, while Cu^{II} retained the signal-to-noise per unit time, suggesting that alternative dopants could be used to optimize experimental performance further.

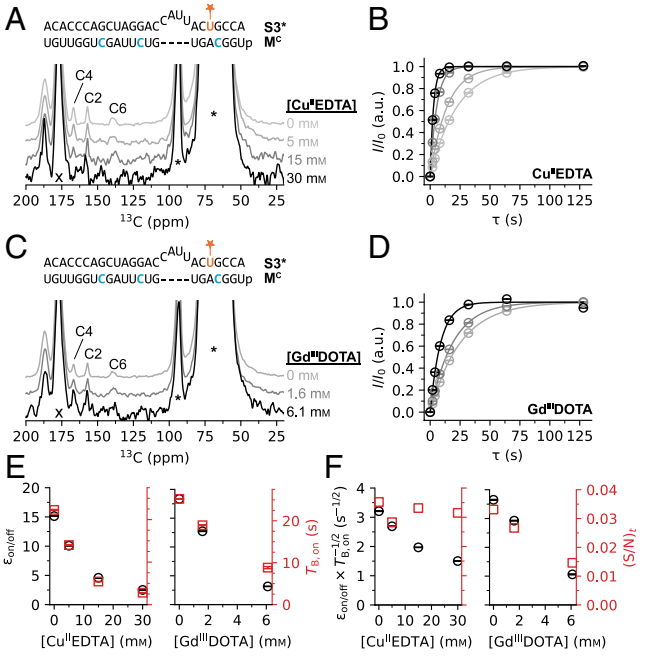

Fig. 4. (*A*) ^{1}H–^{13}C CP MAS spectra (3 ms τ_{CP}) of **M^{C}S3*** in DNP nectar with increasing concentrations of paramagnetic Cu^{II}EDTA. Spectra are scaled to the same max. signal intensity. Asterisks denote background from natural isotopic abundance glycerol, trehalose, and mannitol. x indicates spinning side bands. (*B*) Build-up of bulk ^{1}H polarization for the same samples measured by saturation recovery. $T_{B,on}$ was determined from monoexponential fits to the data (solid lines). (*C* and *D*) Same data for **M^{C}S3*** with added Gd^{III}DOTA. (*E*) Quantification of targeted DNP enhancement factors ($\varepsilon_{on/off}$, black) and bulk ^{1}H polarization build-up times ($T_{B,on}$, red) for the data in panels (*A*–*D*) (*SI Appendix*, Table S5). While addition of paramagnetic metal ions results in a pronounced improvement of $T_{B,on}$, $\varepsilon_{on/off}$ is affected negatively. (*F*) The resulting DNP sensitivities [$\varepsilon_{on/off} \times (T_{B,on})^{-1/2}$, black] did not show reduced sensitivity per unit time upon addition of Cu^{II}, while for Gd^{III}, the signal-to-noise per unit time (red) was reduced.

Spin diffusion in proton-rich matrices spreads polarization between neighboring RNA duplexes. Hence, deuteration of the matrix greatly improved intramolecular localization of the polarization enhancement with only a moderate loss of sensitivity. This approach allows targeted DNP studies of nucleic acids in the same way they have long been possible for proteins, without needing preexisting binding sites for paramagnetic metal ions such as Mn^{2+}, making the method broadly applicable. Moreover, the relatively low effective biradical PA concentration used here (20 to 40 μM, compared with ~10 mM conventional CE DNP) may be advantageous for in-cell applications by minimizing potential unwanted interactions with cellular components.

Materials and Methods

Full details for the synthesis and characterization of **AsymPol-NCS-SDSL**, synthesis, spin-labeling, and EPR analysis of RNA oligonucleotides as well as technical details about MAS DNP NMR instrumentation and experiments are given in *SI Appendix*.

RNA Synthesis and Folding. Sequence information is given in *SI Appendix*, Table S2. All RNAs were purified by denaturing PAGE (77). The purity was checked by analytical denaturing PAGE and concentrations were determined from the ultraviolet absorbance at 260 nm.

In vitro transcription. Unmodified mSirt1 RNA was prepared by in vitro transcription from a synthetic DNA template with T7 RNA polymerase (78). The preparation of miR-34a with nucleotide-specific isotope labeling using cleavage of tandem transcripts with RNase H has been described earlier (5, 79).

Solid-phase synthesis. Amino-modified RNA oligonucleotides were prepared by standard solid-phase synthesis (80, 81) with 2′-*O*-TOM-protected rA^{Ac}, rC^{Ac}, rG^{Ac}, and rU phosphoramidites using 5-ethylthio-1*H*-tetrazole as the activator. 2′-NH_2-modified nucleotides were incorporated as 2′-*N*-TFA protected C^{Bz} and U phosphoramidites.

Spin-labeling with AsymPol-NCS-SDSL. Amino-modified RNA (20 to 40 nmol) was dissolved in borate buffer (20 μL, 100 mM, pH 8.6), mixed with **AsymPol-NCS-SDSL** (20 μL, 100 mM solution in DMF) and incubated at 37 °C for 4 to 8 h. Following PAGE purification, the spin-labeled RNA was analyzed by ESI MS and EPR spectroscopy.

Folding. miR-34a:mSirt1 duplexes were folded by dissolving each RNA (5 nmol) in a buffer containing 15 mM NaP_i pH 6.5, 25 mM NaCl, and 0.1 mM EDTA (20 μL), heating to 95 °C for 5 min and letting cool to 25 °C over the course of 3 h. Proper annealing was confirmed by analytical native PAGE (15%).

Solid-State MAS DNP NMR Spectroscopy.

Sample preparation. Annealed RNA duplexes (5 nmol) were lyophilized and mixed with trehalose and mannitol (9 μL, 500 mM each in H_2O or D_2O), H_2O or D_2O (1 μL), and $^{12}C_3$,$^2H_8$-glycerol or $^2H_8$-glycerol (15 μL). The compositions of all samples are listed in *SI Appendix*, Table S3.

For metal ion titrations, the annealed duplex **M^{C}S3*** (5 nmol) was lyophilized and dissolved in a mixture of trehalose and mannitol (8 μL, 500 mM each in H_2O) and $^2H_8$-glycerol (15 μL). Solutions of $Cu^{II}Na_2EDTA$ (300 mM) or $Gd^{III}DOTA$ (90 mM) were successively added in aliquots of 0.4 to 1.3 μL to achieve the dopant concentrations listed in *SI Appendix*, Table S5.

Samples were transferred into 3.2 mm sapphire rotors, sealed with silicone plugs or polytetrafluoroethylene inserts and closed with VESPEL SP-1 drive caps.

MAS DNP experiments. ^1H–^{13}C CP MAS spectra were acquired with and without μw irradiation for all samples to calculate the DNP enhancement factor $\varepsilon_{on/off}$. Signal intensities ($I_{on/off}$) and root mean square (RMS) of the noise ($\sigma_{on/off}$) were measured from 50 to 110 ppm and 350 to 380 ppm, respectively. Taking into account the number of scans ($NS_{on/off}$) for each experiment, the enhancement factor and its uncertainty are given by

$$\varepsilon_{on/off} = \frac{I_{on}\ NS_{off}}{I_{off}\ NS_{on}}, \quad [1]$$

$$\Delta\varepsilon_{on/off} = \sqrt{\left(\frac{\sigma_{on}}{I_{on}}\right)^2 + \left(\frac{\sigma_{off}}{I_{off}}\right)^2}. \quad [2]$$

Polarization build-up times of the bulk ^1H magnetization under μw irradiation ($T_{B,on}$) were determined via echo saturation recovery (*SI Appendix*, Fig. S2*B*) with eight values between 0 and 128 s for recovery delay τ. Time points were acquired in a single scan after 200 ms saturation and processed with an exponential line broadening of 500 Hz. Integrated bulk ^1H signal intensities were fitted to a mono-exponential function with weights for each time point given by the RMS of the noise in an empty region of the spectrum. Uncertainties of the resulting $T_{B,on}$ were taken as the SE of the fit:

$$I(t) = I_0\left(1 - e^{\frac{t}{T_{B,on}}}\right). \quad [3]$$

Data, Materials, and Software Availability. Study data are included in the article and/or *SI Appendix*.

ACKNOWLEDGMENTS. This work benefited from access to the Center for Biomolecular Magnetic Resonance at the Goethe University in Frankfurt am Main, Germany and has been supported by iNEXT-Discovery (grant number 871037) funded by the Horizon 2020 program of the European Commission. R.D. acknowledges funding from European Union's Horizon 2020 research and innovation program under the Marie Skłodowska-Curie Fellowship (101067627, project: ECONOMICS) and ModernaTX Inc. United States, Global Fellowship for Young Researchers (ID: 2022-70). K.P. acknowledges funding support from Knut and Alice Wallenberg Foundation collaborative project grant (KAW 2016.0087) and Wallenberg Academy fellow grant (2019.0227), Cancerfonden (21 1770 Pj), Swedish research council (2018-00250_VR), and Stiftelse för Strategisk Forskning (FFL15-0178). S.T.S. acknowledges funding from the Icelandic Research Fund (grant number 239662). A.T.W. and S.C. acknowledge PhD fellowships from the University of Iceland Research Fund. T7 polymerase was produced by the Protein Science Facility at Karolinska Institute. SwedNMR National NMR facility at Gothenburg University, Sweden, provided access to the DNP MAS NMR instrument. We thank Dr. Timo Weinrich (Goethe University, Frankfurt am Main, Germany) for ESI-MS analyses of RNA oligonucleotides and Dr. Frederic Mentink-Vigier (MagLab, Florida State University, Tallahassee, United States) for helpful discussions about cross-effect DNP.

Author affiliations: [a]Department of Medical Biochemistry and Microbiology, Science for Life Laboratory, Center of Excellence for the Chemical Mechanisms of Life, Uppsala University, Uppsala 751 23, Sweden; and [b]Department of Chemistry, Science Institute, University of Iceland, Reykjavik 107, Iceland

Author contributions: R.D., C.S., S.T.S., and K.P. designed research; R.D., C.S., A.T.W., S.C., and G.W.R. performed research; A.T.W., S.C., and S.T.S. contributed new reagents/analytic tools; R.D. and C.S. analyzed data; and R.D., C.S., A.T.W., S.C., S.T.S, and K.P. wrote the paper.

1. Y. Peng, C. M. Croce, The role of MicroRNAs in human cancer. *Sig. Transduct. Target. Ther.* **1**, 15004 (2016).
2. L. Baronti *et al.*, Base-pair conformational switch modulates miR-34a targeting of Sirt1 mRNA. *Nature* **583**, 139–144 (2020).
3. D. M. Kosek, E. Banijamali, W. Becker, K. Petzold, E. R. Andersson, Efficient 3′-pairing renders microrna targeting less sensitive to mrna seed accessibility. *Nucleic Acids Res.* **51**, 11162–11177 (2023).
4. L. Sweetapple *et al.*, Sequence, structure, and affinity of miR-34a binding sites determine repression efficacy. *Nucleic Acids Res.* **53**, gkaf633 (2025).
5. R. Dasgupta, W. Becker, K. Petzold, Elucidating microRNA-34a organisation within human argonaute-2 by dynamic nuclear polarisation-enhanced magic angle spinning NMR. *Nucleic Acids Res.* **52**, 11995–12004 (2024).
6. J. Schlagnitweit *et al.*, Observing an antisense drug complex in intact human cells by in-cell NMR spectroscopy. *ChemBioChem* **20**, 2474–2478 (2019).
7. F.-X. Theillet, In-cell structural biology by NMR: The benefits of the atomic scale. *Chem. Rev.* **122**, 9497–9570 (2022).
8. F.-X. Theillet, E. Luchinat, In-cell NMR: Why and how? *Prog. Nucl. Magn. Reson. Spectrosc.* **132–133**, 1–112 (2022).
9. P. Viskova, D. Krafcik, L. Trantirek, S. Foldynova-Trantirkova, In-cell NMR spectroscopy of nucleic acids in human cells. *Curr. Protoc. Nucleic Acid Chem.* **76**, e71 (2019).
10. S. Foldynova-Trantirkova, J. Harnos, J. Rynes, V. Zlinska, L. Trantirek, In-cell NMR spectroscopy of nucleic acids: Basic concepts, practical aspects, and applications. *Prog. Nucl. Magn. Reson. Spectrosc.* **148–149**, 101560 (2025).

11. H. T. P. Annecke *et al.*, Optimising in-cell NMR acquisition for nucleic acids. *J. Biomol. NMR* **78**, 249–264 (2024).
12. V. Aladin, A. K. Sreemantula, T. Biedenbänder, A. Marchanka, B. Corzilius, Specific signal enhancement on an RNA-protein interface by dynamic nuclear polarization. *Chem. Eur. J.* **29**, e202203443 (2023).
13. A. Equbal, A. Leavesley, S. K. Jain, S. Han, Cross-effect dynamic nuclear polarization explained: Polarization, depolarization, and oversaturation. *J. Phys. Chem. Lett.* **10**, 548–558 (2019).
14. A. S. Lilly Thankamony, J. J. Wittmann, M. Kaushik, B. Corzilius, Dynamic nuclear polarization for sensitivity enhancement in modern solid-state NMR. *Prog. Nucl. Magn. Reson. Spectrosc.* **102–103**, 120–195 (2017).
15. M. Kaplan *et al.*, Probing a cell-embedded megadalton protein complex by DNP-supported solid-state NMR. *Nat. Methods* **12**, 649–652 (2015).
16. A. König *et al.*, Hyperpolarized MAS NMR of unfolded and misfolded proteins. *Solid State Nucl. Magn. Reson.* **98**, 1–11 (2019).
17. B. Uluca *et al.*, DNP-enhanced MAS NMR: A tool to snapshot conformational ensembles of α-synuclein in different states. *Biophys. J.* **114**, 1614–1623 (2018).
18. D. W. Conroy *et al.*, Probing Watson-Crick and Hoogsteen base pairing in duplex DNA using dynamic nuclear polarization solid-state NMR spectroscopy. *Proc. Natl. Acad. Sci. U.S.A.* **119**, e2200681119 (2022).
19. L. Bhai *et al.*, Hydrogen bonding in duplex DNA probed by DNP enhanced solid-state NMR N–H bond length measurements. *Front. Mol. Biosci.* **10**, 1286172 (2023).
20. T. Wiegand *et al.*, Protein–nucleotide contacts in motor proteins detected by DNP–enhanced solid-state NMR. *J. Biomol. NMR* **69**, 157–164 (2017).
21. S. Narasimhan *et al.*, DNP-supported solid-state NMR spectroscopy of proteins inside mammalian cells. *Angew. Chem. Int. Ed. Engl.* **58**, 12969–12973 (2019).
22. D. Beriashvili *et al.*, A high-field cellular DNP-supported solid-state NMR approach to study proteins with sub-cellular specificity. *Chem. Sci.* **14**, 9892–9899 (2023).
23. W. N. Costello, Y. Xiao, F. Mentink-Vigier, J. Kragelj, K. K. Frederick, DNP-assisted solid-state NMR enables detection of proteins at nanomolar concentrations in fully protonated cellular milieu. *J. Biomol. NMR* **78**, 95–108 (2024).
24. M. D. Kraffčíková *et al.*, A DNP-supported solid-state NMR approach to study nucleic acids in situ reveals berberine-stabilized Hoogsteen structures in mitochondria. *Angew. Chem. Int. Ed. Engl.* **64**, e202424131 (2025).
25. B. J. Albert *et al.*, Dynamic nuclear polarization nuclear magnetic resonance in human cells using fluorescent polarizing agents. *Biochemistry* **57**, 4741–4746 (2018).
26. Y. Rao *et al.*, An efficient and stable polarizing agent for in-cell magic-angle spinning dynamic nuclear polarization NMR spectroscopy. *J. Phys. Chem. Lett.* **15**, 11601–11607 (2024).
27. P. S. Nadaud, J. J. Helmus, N. Höfer, C. P. Jaroniec, Long-range structural restraints in spin-labeled proteins probed by solid-state nuclear magnetic resonance spectroscopy. *J. Am. Chem. Soc.* **129**, 7502–7503 (2007).
28. P. Rovó, K. Grohe, K. Giller, S. Becker, R. Linser, Proton transverse relaxation as a sensitive probe for structure determination in solid proteins. *ChemPhysChem* **16**, 3791–3796 (2015).
29. E. A. W. Van Der Cruijsen *et al.*, Biomolecular DNP-supported NMR spectroscopy using site-directed spin labeling. *Chem. Eur. J.* **21**, 12971–12977 (2015).
30. M. A. Voinov *et al.*, Cysteine-specific labeling of proteins with a nitroxide biradical for dynamic nuclear polarization NMR. *J. Phys. Chem. B* **119**, 10180–10190 (2015).
31. T. Viennet *et al.*, Selective protein hyperpolarization in cell lysates using targeted dynamic nuclear polarization. *Angew. Chem. Int. Ed. Engl.* **55**, 10746–10750 (2016).
32. B. J. Lim, B. E. Ackermann, G. T. Debelouchina, Targetable tetrazine-based dynamic nuclear polarization agents for biological systems. *ChemBioChem* **21**, 1315–1319 (2020).
33. R. Rogawski *et al.*, Dynamic nuclear polarization signal enhancement with high-affinity biradical tags. *J. Phys. Chem. B* **121**, 1169–1175 (2017).
34. I. Marin-Montesinos *et al.*, Selective high-resolution DNP-enhanced NMR of biomolecular binding sites. *Chem. Sci.* **10**, 3366–3374 (2019).
35. M. Kaushik *et al.*, Gd(iii) and Mn(ii) complexes for dynamic nuclear polarization: Small molecular chelate polarizing agents and applications with site-directed spin labeling of proteins. *Phys. Chem. Chem. Phys.* **18**, 27205–27218 (2016).
36. J. Heiliger *et al.*, Site-specific dynamic nuclear polarization in a Gd(III)-labeled protein. *Phys. Chem. Chem. Phys.* **22**, 25455–25466 (2020).
37. P. Wenk *et al.*, Dynamic nuclear polarization of nucleic acid with endogenously bound manganese. *J. Biomol. NMR* **63**, 97–109 (2015).
38. D. Daube, M. Vogel, B. Suess, B. Corzilius, Dynamic nuclear polarization on a hybridized hammerhead ribozyme: An explorative study of RNA folding and direct DNP with a paramagnetic metal ion cofactor. *Solid State Nucl. Magn. Reson.* **101**, 21–30 (2019).
39. B. Fazliji, C. Ferreira Rodrigues, H. Wang, R. K. O. Sigel, "2.20–Metal ion interactions with nucleic acids" in *Comprehensive Inorganic Chemistry III*, J. Reedijk, K. R. Poeppelmeier, Eds. (Elsevier, ed. 3, 2023), pp. 629–663.
40. G. Menzildjian *et al.*, Polarizing agents for efficient high field DNP solid-state NMR spectroscopy under magic-angle spinning: From design principles to formulation strategies. *Chem. Sci.* **14**, 6120–6148 (2023).
41. L. Niccoli *et al.*, Efficient DNP at high fields and fast MAS with antenna-sensitized dinitroxides. *Chem. Sci.* **15**, 16582–16593 (2024).
42. R. Wei *et al.*, Systematic evaluation of polarizing agents for dynamic nuclear polarization enhanced NMR. *Angew. Chem. Int. Ed. Engl.* **64**, e202505944 (2025), 10.1002/anie.202505944.
43. J. S. Tregoning, N. N. Sanders, The past, present, and future of RNA vaccines. *Mol. Ther.* **33**, 1876–1878 (2025).
44. S. Oliveto, N. Manfrini, S. Biffo, The power of microrna regulation—Insights into immunity and metabolism. *FEBS Lett.* **599**, 1821–1851 (2025).
45. F. Mentink-Vigier *et al.*, Computationally assisted design of polarizing agents for dynamic nuclear polarization enhanced NMR: The AsymPol family. *J. Am. Chem. Soc.* **140**, 11013–11019 (2018).
46. S. Saha, A. P. Jagtap, STh. Sigurdsson, Site-directed spin labeling of 2′-amino groups in RNA with isoindoline nitroxides that are resistant to reduction. *Chem. Commun.* **51**, 13142–13145 (2015).
47. S. Hediger, D. Lee, F. Mentink-Vigier, G. De Paëpe, MAS-DNP enhancements: Hyperpolarization, depolarization, and absolute sensitivity. *eMagRes* **7**, 105–116 (2018).
48. P. M. Gordon *et al.*, New strategies for exploring RNA's 2′-OH expose the importance of solvent during group II intron catalysis. *Chem. Biol.* **11**, 237–246 (2004).
49. J. L. Hougland, J. A. Piccirilli, "Chapter 6–2′-amino-modified ribonucleotides as probes for local interactions within RNA" in *Biophysical, Chemical, and Functional Probes of RNA Structure, Interactions and Folding: Part A* (*Methods in Enzymology*, Academic Press, 2009), vol. 468, pp. 107–125.
50. S. T. Sigurdsson, T. Tuschl, F. Eckstein, Probing RNA tertiary structure: Interhelical crosslinking of the hammerhead ribozyme. *RNA* **1**, 575–583 (1995).
51. Q. Dai, S. K. Deb, J. L. Hougland, J. A. Piccirilli, Improved synthesis of 2′-amino-2′-deoxyguanosine and its phosphoramidite. *Bioorg. Med. Chem.* **14**, 705–713 (2006).
52. C. Falschlunger, R. Micura, Efficient access to N-trifluoroacetylated 2′-amino-2′-deoxyadenosine phosphoramidite for RNA solid-phase synthesis. *Monatsh. Chem.* **150**, 795–800 (2019).
53. S. Moreno, J. M. R. Pittol, M. Hartl, R. Micura, Robust synthesis of 2′-azido modified RNA from 2′-amino precursors by diazotransfer reaction. *Org. Biomol. Chem.* **20**, 7845–7850 (2022).
54. R. Padilla, R. Sousa, Efficient synthesis of nucleic acids heavily modified with non-canonical ribose 2′-groups using a mutant T7 RNA polymerase (RNAP). *Nucleic Acids Res.* **27**, 1561–1563 (1999).
55. S. Sato *et al.*, Synthesis and spectral properties of polymethine-cyanine dye–nitroxide radical hybrid compounds for use as fluorescence probes to monitor reducing species and radicals. *Spectrochim. Acta A Mol. Biomol. Spectrosc.* **71**, 2030–2039 (2009).
56. J. R. Brender *et al.*, Trehalose as an alternative to glycerol as a glassing agent for in vivo DNP MRI. *Magn. Reson. Med.* **85**, 42–48 (2021).
57. A. Leavesley *et al.*, Maximizing NMR signal per unit time by facilitating the e–e–n cross effect DNP rate. *Phys. Chem. Chem. Phys.* **20**, 27646–27657 (2018).
58. Y. Li, A. Equbal, K. Tagami, S. Han, Electron spin density matching for cross-effect dynamic nuclear polarization. *Chem. Commun.* **55**, 7591–7594 (2019).
59. A. Equbal *et al.*, Role of electron spin dynamics and coupling network in designing dynamic nuclear polarization. *Prog. Nucl. Magn. Reson. Spectrosc.* **126–127**, 1–16 (2021).
60. C. Tobar *et al.*, Multi electron spin cluster enabled dynamic nuclear polarization with sulfonated BDPA. *J. Phys. Chem. Lett.* **14**, 11640–11650 (2023).
61. R. K. Chaklashiya *et al.*, Dynamic nuclear polarization using electron spin cluster. *J. Phys. Chem. Lett.* **15**, 5366–5375 (2024).
62. C. P. Jaroniec, C. Filip, R. G. Griffin, 3D TEDOR NMR experiments for the simultaneous measurement of multiple carbon−nitrogen distances in uniformly ^{13}C, ^{15}N-labeled solids. *J. Am. Chem. Soc.* **124**, 10728–10742 (2002).
63. R. R. Ernst *et al.*, *Principles of Nuclear Magnetic Resonance in One and Two Dimensions* (Oxford University Press, 1990).
64. B. Corzilius, L. B. Andreas, A. A. Smith, Q. Z. Ni, R. G. Griffin, Paramagnet induced signal quenching in MAS–DNP experiments in frozen homogeneous solutions. *J. Magn. Reson.* **240**, 113–123 (2014).
65. W.-M. Yau, J. Jeon, R. Tycko, Succinyl-DOTOPA: An effective triradical dopant for low-temperature dynamic nuclear polarization with high solubility in aqueous solvent mixtures at neutral pH. *J. Magn. Reson.* **311**, 106672 (2020).
66. J. Becker-Baldus *et al.*, Probing the conformational space of the cannabinoid receptor 2 and a systematic investigation of DNP-enhanced MAS NMR spectroscopy of proteins in detergent micelles. *ACS Omega* **8**, 32963–32976 (2023).
67. D. J. Cheney, P. C. Vioglio, A. Brookfield, F. Blanc, Optimisation of dynamic nuclear polarisation using "off-the-shelf" Gd(III)-based polarising agents. *Phys. Chem. Chem. Phys.* **26**, 24395–24406 (2024).
68. F. J. Scott, S. Eddy, T. Gullion, F. Mentink-Vigier, Sorbitol-based glass matrices enable dynamic nuclear polarization beyond 200 K. *J. Phys. Chem. Lett.* **15**, 8743–8751 (2024).
69. S. Chatterjee, F. J. Scott, STh. Sigurdsson, A. Venkatesh, F. Mentink-Vigier, Indirect detection of the protons in and around biradicals and their mechanistic role in MAS-DNP. *J. Phys. Chem. Lett.* **16**, 635–641 (2025).
70. G. Stevanato *et al.*, Open and closed radicals: Local geometry around unpaired electrons governs magic-angle spinning dynamic nuclear polarization performance. *J. Am. Chem. Soc.* **142**, 16587–16599 (2020).
71. K. R. Thurber, R. Tycko, Theory for cross effect dynamic nuclear polarization under magic-angle spinning in solid state nuclear magnetic resonance: The importance of level crossings. *J. Chem. Phys.* **137**, 084508 (2012).
72. S. Chatterjee, A. Venkatesh, S. Th. Sigurdsson, F. Mentink-Vigier, Role of protons in and around strongly coupled nitroxide biradicals for cross-effect dynamic nuclear polarization. *J. Phys. Chem. Lett.* **15**, 2160–2168 (2024).
73. M. M. Rosay, *"Sensitivity-enhanced nuclear magnetic resonance of biological solids,"* PhD thesis, Massachusetts Institute of Technology, Boston, MA, (2001).
74. A. Capozzi *et al.*, Gadolinium effect at high-magnetic-field DNP: 70% ^{13}C polarization of [U-^{13}C] glucose using trityl. *J. Phys. Chem. Lett.* **10**, 3420–3425 (2019).
75. N. P. Wickramasinghe *et al.*, Nanomole-scale protein solid-state NMR by breaking intrinsic 1H T1 boundaries. *Nat. Methods* **6**, 215–218 (2009).
76. B. Corzilius, A. A. Smith, R. G. Griffin, Solid effect in magic angle spinning dynamic nuclear polarization. *J. Chem. Phys.* **137**, 054201 (2012).
77. A. Petrov, T. Wu, E. V. Puglisi, J. D. Puglisi, "Chapter seventeen–RNA purification by preparative polyacrylamide gel electrophoresis" in Laboratory Methods in Enzymology in *(Methods in Enzymology*, (Academic Press, 2013), vol. 530, pp. 315–330.
78. L. Baronti, H. Karlsson, M. Marušič, K. Petzold, A guide to large-scale RNA sample preparation. *Anal. Bioanal. Chem.* **410**, 3239–3252 (2018).
79. H. Feyrer, R. Munteanu, L. Baronti, K. Petzold, One-pot production of RNA in high yield and purity through cleaving tandem transcripts. *Molecules* **25**, 1142 (2020).
80. N. Rublack *et al.*, Synthesis of specifically modified oligonucleotides for application in structural and functional analysis of RNA. *J. Nucleic Acids* **2011**, 805253 (2011).
81. L. Flemmich, R. Bereiter, R. Micura, Chemical synthesis of modified RNA. *Angew. Chem. Int. Ed. Engl.* **63**, e202403063 (2024).